Dalton Transactions

ROYAL SOCIETY OF CHEMISTRY

PAPER

View Article Online
View Journal | View Issue

Cite this: *Dalton Trans.*, 2025, **54**, 9296

V doped hollow Co_3O_4 nanoprisms with a modulated electronic structure for high-performance oxygen evolution reaction†

Yanqiang Li,[a] Junyan Chen,[b] Haojie Dong,[a] Zineng Dong,[a] Chenxi Zhang*[a] and Siru Chen *[b]

Received 3rd April 2025,
Accepted 13th May 2025

DOI: 10.1039/d5dt00800j

rsc.li/dalton

The sluggish oxygen evolution reaction (OER) kinetics in water splitting makes it crucial to design highly active OER catalysts. Spinel oxides are considered as promising candidates due to their various compositions, valence states and electronic configurations. This paper reports a facile procedure to prepare V-doped hollow Co_3O_4 nanoprisms for the OER. The introduction of V can effectively modulate the electronic structure of Co_3O_4, therefore improving its intrinsic catalytic activity. The hollow prismatic structure ensures the exposure of catalytically active sites and rapid mass transport, thereby improving the extrinsic catalytic activity. As a result, optimized V-Co_3O_4-5 exhibits a small overpotential of 288 mV at 10 mA cm^{-2} with good durability. This work provides an innovative direction for designing efficient OER electrocatalysts *via* heteroatom doping.

1. Introduction

Hydrogen has long been considered as a promising sustainable energy source due to its renewability.[1,2] It holds significant potential for reducing dependence on fossil fuel and addressing global climate change.[3,4] Electrocatalytic water splitting technology is considered as a green and sustainable method for hydrogen production, and attracts significant attention.[5,6] In theory, H_2O can be completely decomposed into H_2 and O_2 at a thermodynamic potential of 1.23 V. Due to the slow four-electron transfer process, the anodic oxygen evolution reaction (OER) is the bottleneck for overall water splitting.[7–9] To address the sluggish kinetics and improve OER efficiency, noble metal oxides like RuO_2 and IrO_2 are widely employed to reduce the overpotential of the OER.[10,11] However, their widespread application is constrained by their high cost, low abundance, and limited stability. Therefore, more efforts are needed for large-scale production of non-noble metal-based catalysts with both high activity and stability.[12–15]

Recently, transition metal catalysts have been widely investigated for the OER, including oxides/hydroxides, sulfides, nitrides, phosphides, and borides. Among these, transition metal oxides are prized for their low cost, high stability, adjustable chemical composition, and lattice oxygen.[16–20] Spinel oxides, with a formula of AB_2O_4, attract specific attention owing to the dual active sites in the crystal structure and the diverse oxidation states of transition metal cations.[21–23] Spinel-type oxide Co_3O_4, where Co^{2+} and Co^{3+} occupy tetrahedral and octahedral sites, respectively, is one of the most investigated spinel oxides for the OER.[24–26] For example, by integrating metal vacancies and tensile strain into Co_3O_4, Guo *et al.* prepared Co_3O_4 with a small overpotential of 327 mV at 10 mA cm^{-2}.[27]

To further improve the catalytic activity of Co_3O_4, different strategies such as morphology engineering, defect engineering, and heteroatom doping have been applied. Heteroatom doping can improve the intrinsic catalytic activity of Co_3O_4 *via* optimizing the adsorption energy of intermediates, adjusting the electronic structure of metal active sites and reducing the reaction barrier.[28–32] For example, by introducing highly active W sites into Co_3O_4, W-Co_3O_4 prepared by Cao *et al.* exhibited a small overpotential of 251 mV at 10 mA cm^{-2}.[33] Li *et al.* prepared Nd and Ni co-doped Co_3O_4 and found that Ni could induce the formation of CoOOH and Nd could reduce the barrier for the formation of CoOOH, therefore leading to improved catalytic activity.[34] In addition, recent works have demonstrated that V doping can improve the catalytic activity of electrocatalysts such as Ni_2P and CoP_2 by promoting the

[a]*School of Materials Science and Engineering, North China University of Water Resources and Electric Power, Zhengzhou, 450045, China.*
E-mail: zhangchenxi@ncwu.edu.cn
[b]*School of Material and Chemical Engineering, Center for Advanced Materials Research, Zhongyuan University of Technology, Zhengzhou, 450007, China.*
E-mail: siruchen@zut.edu.cn

†Electronic supplementary information (ESI) available. See DOI: https://doi.org/10.1039/d5dt00800j

formation of NiOOH and Co_3O_4, while the role of V should be further investigated.[35,36]

On the other hand, designing an appropriate nanostructure can improve the extrinsic catalytic activity. Firstly, a regular nanostructure can induce the effective exposure of catalytically active sites. Secondly, by designing catalysts with high specific area, the mass transport can also be promoted.[37–39] In addition, it has been proposed that the electronic structure such as the d band center of catalysts can also be optimized by size/morphology engineering.[40,41]

Based on the advantage of spinel oxides and regular nanocatalysts, in this work, we report a facile method to prepare V doped Co_3O_4 (V-Co_3O_4) with a hollow prismatic structure. The hollow features ensure the exposure of active sites as well as electron/reactant transport and gas release. V doping induces the formation of oxygen vacancies in low coordination sites and regulates the electronic structure of Co_3O_4, therefore improving the conductivity and intrinsic catalytic activity of Co_3O_4. Optimized V-Co_3O_4-5 exhibits an overpotential of 288 mV at 10 mA cm^{-2}, a Tafel slope of 65.43 mV dec^{-1}, and good durability for more than 90 hours, demonstrating its practical application.

2. Experimental

2.1 Preparation of Co precursors

0.75 g of cobalt acetate tetrahydrate and 2 g of PVP (MW. 58 000) were dissolved in 100 ml ethanol. After refluxing at 85 °C for 4 h, the product was filtered and washed using ethanol. The product was dried at 60 °C overnight.

2.2 Preparation of V-Co_3O_4

0.04 g of Co precursor was dispersed in 40 ml ethanol, and then a certain amount of sodium orthovanadate (Na_3VO_4) in 10 ml water was added. The solution was stirred for two hours at room temperature. Afterwards, the obtained product was filtered and washed using ethanol. After drying at 60 °C, the materials were calcined at 400 °C for 2 hours to obtained V-Co_3O_4. By changing the amount of sodium orthovanadate (0 mg, 5 mg, 10 mg and 20 mg), the obtained catalysts are denoted as Co_3O_4, V-Co_3O_4-5, V-Co_3O_4-10, and V-Co_3O_4-20 respectively.

3. Results and discussion

As shown in Fig. 1, a series of V-Co_3O_4-*M* (*M* = 5, 10, 20) were prepared using Na_3VO_4 as the vanadium source and a cobalt-based nanoprism as the template. The composition of the cobalt-based nanoprism is $Co_5(OH)_2(Ac)_8{\cdot}2H_2O$, which has been well demonstrated in previous literature reports.[40,42] During reaction with Na_3VO_4, ion-exchange reaction occurs and due to the Kirkendall effect, hollow $CoVO_x$ is achieved. After calcinating at 400 °C in air, V doped Co_3O_4 was successfully prepared. SEM images demonstrate the structural

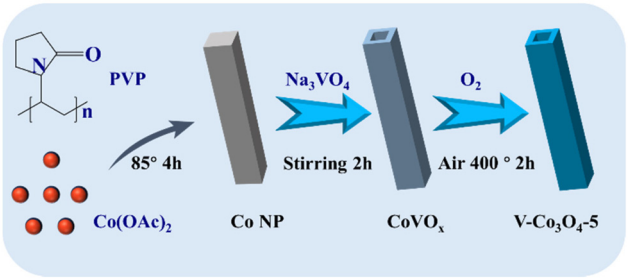

Fig. 1 Schematic illustration of the synthesis of V doped Co_3O_4.

change, where the Co precursor exhibits a prismatic structure with a length of 1 μm and a width of 0.5 μm (Fig. 2a). After calcination of the Co precursor, the obtained Co_3O_4 exhibits agglomerated nanoparticles due to its decomposition (Fig. S1†). However, the morphology of V-Co_3O_4 is well preserved, except that the surface becomes rough and the interior becomes hollow (Fig. 2b, c, Fig. S2 and S3†). This is due to the formation of rigid $CoVO_x$ by the reaction of the Co precursor with Na_3VO_4, which can preserve the framework during the calcination process. The hollow structure can improve the specific surface area of V-Co_3O_4, as demonstrated by the N_2 adsorption–desorption isotherms in Fig. S4.† The N_2 uptake of V-Co_3O_4 is obviously higher than that of Co_3O_4, and the calculated Brunauer–Emmett–Teller (BET) specific surface areas are 105 and 50 $m^2\ g^{-1}$ for V-Co_3O_4 and Co_3O_4, respectively. The pore size distribution curves demonstrate the existence of micropores at 1 nm and mesopores between 7 and 15 nm for V-Co_3O_4. This hollow structure with high specific surface area can enhance the contact between the electrocatalyst and the electrolyte, thereby boosting the OER. The hollow structure was further demonstrated by the TEM image (Fig. 2d). In addition, the lattice distances of 2.43 and 2.85 nm can be attributed to the (311) and (220) planes of Co_3O_4 (Fig. 2e). The diffraction rings shown in Fig. 2f further demonstrate the formation of Co_3O_4. Energy-dispersive X-ray spectroscopy (EDX) elemental mapping of V-Co_3O_4-5 demonstrates the uniform distribution of Co, V, and O elements (Fig. 2g).

X-ray powder diffraction (XRD) was employed to further characterize the structures of Co_3O_4 and V-Co_3O_4. The XRD patterns of prepared Co_3O_4, V-Co_3O_4-5, V-Co_3O_4-10, and V-Co_3O_4-20 exhibit nearly identical patterns, indicating that the doping of vanadium does not alter the crystal phase structure of Co_3O_4 (Fig. 3a). The diffraction peaks located at 31.3°, 36.8°, 59.4°, and 65.2° correspond well to the (220), (311), (511), and (440) planes of cubic spinel Co_3O_4 (PDF#42-1467).[43]

To investigate the surface composition and valence state information of V-doped Co_3O_4 samples, XPS measurements were conducted on Co_3O_4 and V-Co_3O_4. As shown in Fig. S5,† apparent characteristic peaks corresponding to Co, V, and O in V-Co_3O_4-5 were observed, further confirming the successful preparation of V-Co_3O_4.

Specifically, for V-Co_3O_4-5, the Co 2p XPS spectrum exhibits spin–orbit split peaks of Co $2p_{1/2}$ and Co $2p_{3/2}$, indicating

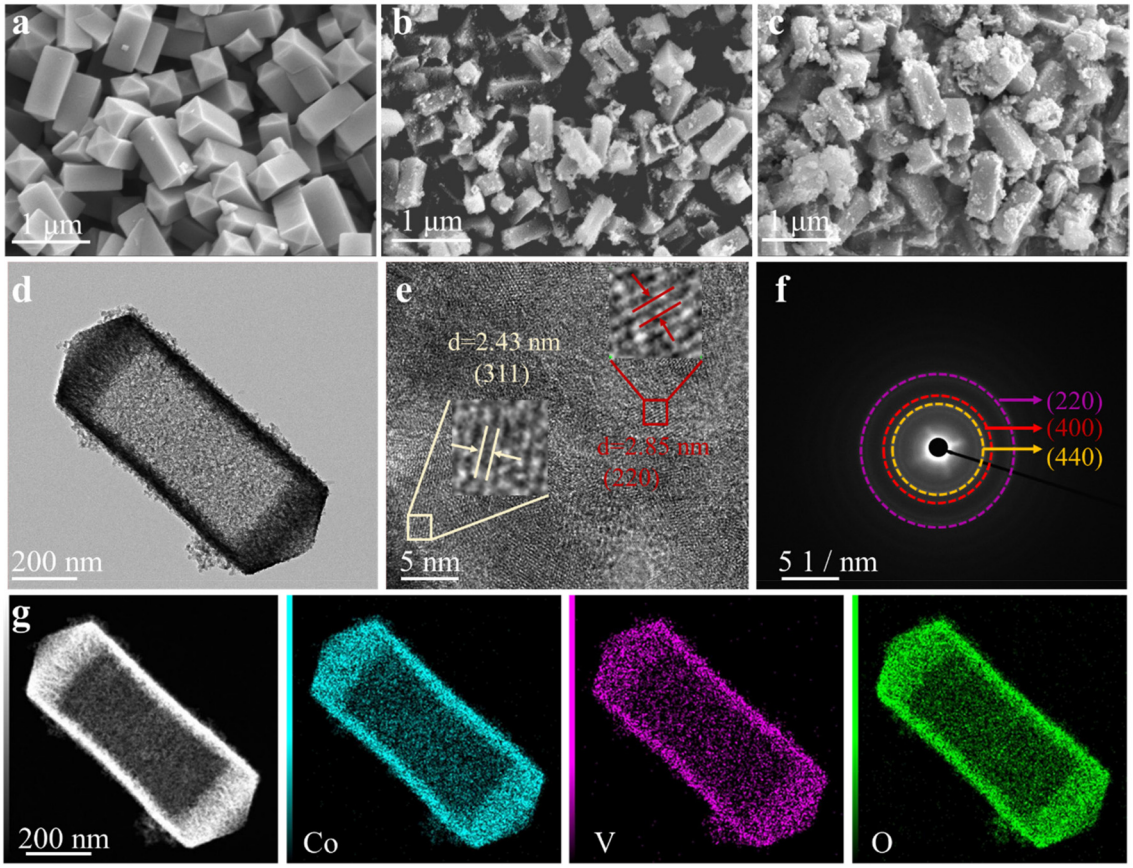

Fig. 2 (a–c) SEM images of the Co precursor, $CoVO_x$ and V-Co_3O_4-5. (d–f) TEM and HRTEM images, and diffraction rings of V-Co_3O_4-5. (g) Element mapping of V-Co_3O_4-5.

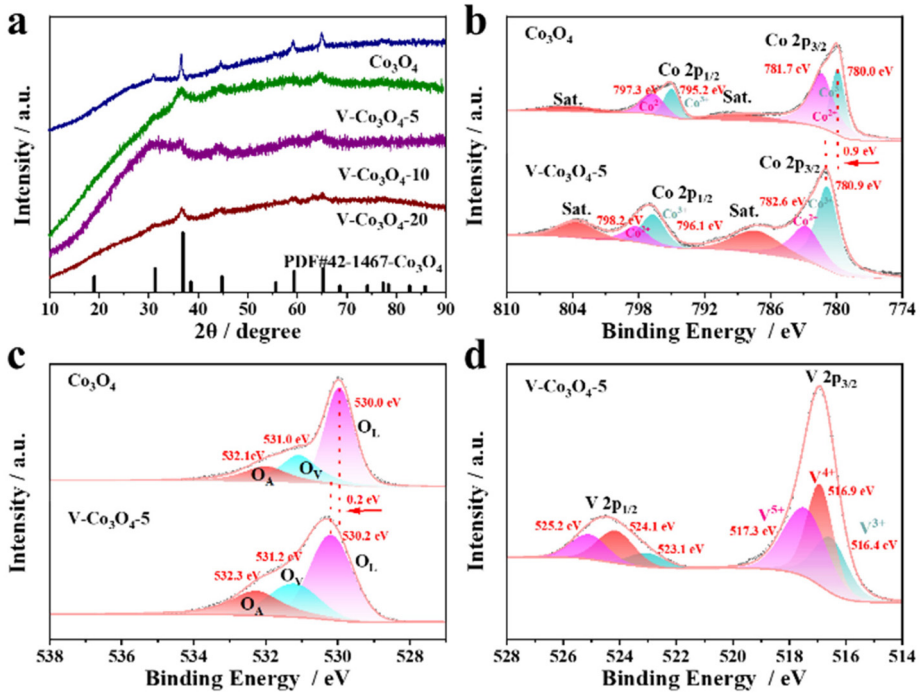

Fig. 3 (a) XRD patterns of Co_3O_4 and V-Co_3O_4. (b and c) Co 2p and O 1s spectra of Co_3O_4 and V-Co_3O_4-5. (d) V 2p spectra of V-Co_3O_4-5.

binding energies of 780.9 eV and 796.1 eV for Co^{3+} and 782.6 eV and 798.2 eV for Co^{2+}, respectively (Fig. 3b). In contrast, the peaks corresponding to Co_3O_4 appear at slightly lower binding energies, specifically 780.0 eV and 795.2 eV for Co^{3+} and 781.7 eV and 797.3 eV for Co^{2+}.[44] It is noteworthy that upon V doping, the peaks corresponding to Co $2p_{1/2}$ and Co $2p_{3/2}$ in V-Co_3O_4-5 shifted positively by 0.9 eV. This indicates that the addition of V effectively tunes the electronic structure of Co in Co_3O_4, leading to more high valent Co species, and high valent Co species have been demonstrated to be highly active catalytic centers for the OER.

In O 1s spectra, peaks located around 530.2, 531.2, and 532.3 eV can be attributed to lattice oxygen (Lo), oxygen vacancies in low coordination sites (O_V), and adsorbed oxygen, respectively (Fig. 3c). Compared to Co_3O_4, the O 1s peaks in V-Co_3O_4 also shift towards higher binding energies, indicating the formation of O_V on the Co_3O_4 surface, which induces new defect states near the bandgap.[45] Electrons localized on oxygen vacancies are easily excited to the conduction band, thereby promoting the electronic conductivity of the electrocatalyst. To further confirm the oxygen vacancies in V-Co_3O_4, electron paramagnetic resonance (EPR) characterization was performed. As shown in Fig. S6,† the EPR spectrum of both Co_3O_4 and V-Co_3O_4 exhibit a symmetric peak at $g = 2.004$, indicating the presence of abundant oxygen vacancies in the catalysts. However, the intensity of the oxygen vacancy peak in V-Co_3O_4 is obviously higher than that in Co_3O_4, suggesting a higher concentration of oxygen vacancies in V-Co_3O_4.[46,47]

The high-resolution V 2p spectrum of V-Co_3O_4-5 can be divided into V $2p_{3/2}$ and V $2p_{1/2}$ regions (Fig. 3d). The V $2p_{3/2}$ region shows peaks at 516.4, 516.9, and 517.3 eV, while V $2_{p1/2}$ exhibits peaks at 523.1, 524.1, and 525.2 eV, corresponding to V^{3+}, V^{4+}, and V^{5+}, respectively.[48] This indicates the coexistence of V^{3+}, V^{4+}, and V^{5+} in V-Co_3O_4-5.

In a word, the XPS results not only demonstrate the formation of Co_3O_4, but also indicate the optimized electronic structure of V-Co_3O_4-5, which is responsible for its improved electrocatalytic performance shown below.

A traditional three-electrode system is used to assess the OER performance of the catalysts. For comparison, the catalytic performance of RuO_2 is also measured under identical testing conditions. Their linear sweep voltammetry (LSV) curves are shown in Fig. 4a. V-Co_3O_4-5 exhibits a 288 mV overpotential at 10 mA cm^{-2}, which is significantly lower than that of Co_3O_4 (367 mV). Similarly, at a high current density of 100 mA cm^{-2}, the overpotential of V-Co_3O_4-5 (360 mV) is also much lower than that of undoped Co_3O_4 (471 mV) (Fig. 4b). This indicates that V-Co_3O_4-5 exhibits superior catalytic activity, highlighting the beneficial effect of V doping. It is worth noting that among these reported non-precious metal OER catalysts, the V-Co_3O_4-5 catalyst exhibits a relatively low overpotential (Table S1†), demonstrating outstanding OER performance.[49–56]

Based on polarization curves, Tafel slopes were calculated to investigate their electrocatalytic kinetics using $\eta = b \log j + a$, where j is the current density and b is the Tafel slope (Fig. 4c). The Tafel slopes for Co_3O_4, V-Co_3O_4-10, and V-Co_3O_4-20 are 71.16 mV dec^{-1}, 70.28 mV dec^{-1}, and 71.48 mV dec^{-1}. However, for V-Co_3O_4-5, the Tafel slope is only 65.43 mV dec^{-1}, significantly lower than those of other comparative samples, indicating faster reaction kinetics. The small Tafel slope indicates fast current increase with the increase of potential, and this is also demonstrated by the increased overpotential from 10 to 100 mA cm^{-2} (Fig. 4b). With the current density increase

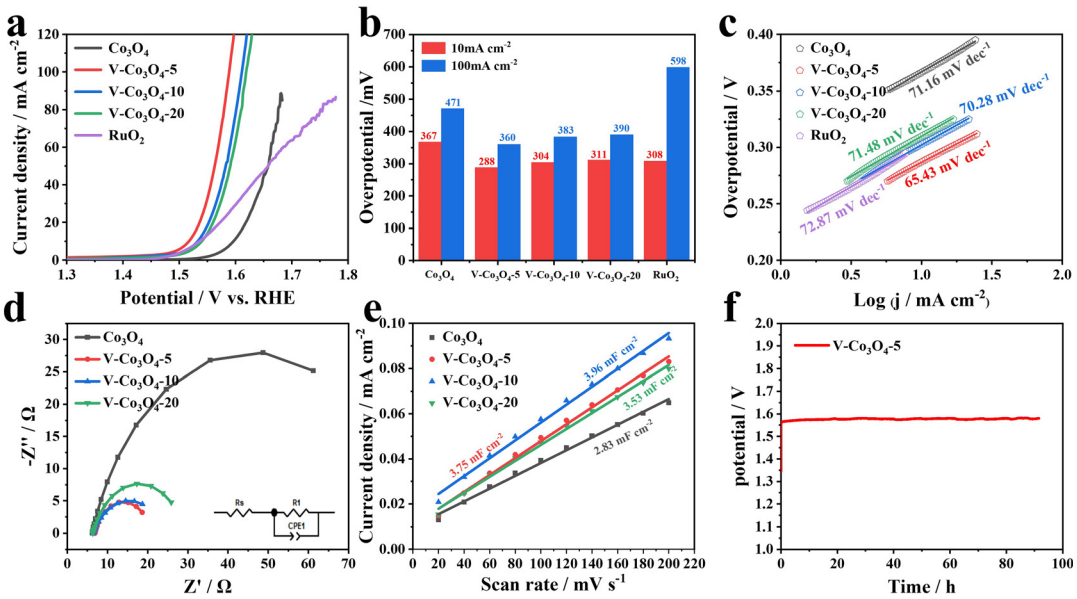

Fig. 4 Electrocatalytic performance of the catalysts. (a) LSV polarization curves in 1.0 M KOH. (b) Overpotentials at 10 and 100 mA cm^{-2}. (c) Tafel slopes. (d) Nyquist plots. (e) C_{dl} values derived from CV curves. (f) Stability of V-Co_3O_4-5 for the OER.

from 10 to 100 mA cm^{-2}, the increased overpotential is the smallest for V-Co_3O_4-5, indicating its potential at large current density.

Electrochemical Impedance Spectroscopy (EIS) was used to test the kinetics and charge carrier migration resistance at the electrolyte/electrode interface (Fig. 4d). A model of an equivalent circuit consisting of one current-induced resistance (R_s), one constant-phase impedance (CPE) and one charge-transfer resistance (R_1) is used to fit the Nyquist plots. Typically, the conductivity of a sample can be reflected by the semicircle of the Nyquist plots. A smaller diameter semicircle indicates a higher conductivity of the sample.[57] The Nyquist plots show that V-Co_3O_4-5 exhibits the lowest charge transfer resistance, indicating that V doping can enhance electron transfer.

It is well-known that the double-layer capacitance (C_{dl}) is directly proportional to the electrochemically active surface area (ECSA), which is another crucial parameter to access the catalytic performance of catalysts. C_{dl} can be derived by cyclic voltammetry at the non-faradaic region (Fig. S7†). As shown in Fig. 4e, it can be observed that the C_{dl} of V-doped Co_3O_4 is significantly higher than that of undoped Co_3O_4, indicating that V doping can increase the ECSA, probably due to the formation of a hollow structure. Higher ECSA can ensure the effective exposure of active sites, thereby improving the catalytic activity.[58,59]

To assess the potential of the V-Co_3O_4-5 catalyst in practical applications, its long-term stability was tested using chronopotentiometry test at 10 mA cm^{-2} by loading V-Co_3O_4-5 on Ni foam. In Fig. 4f, V-Co_3O_4-5 can maintain its catalytic performance for at least 80 hours without degradation, indicating good stability of V-Co_3O_4-5. To investigate phase stability and morphology retention of V-Co_3O_4, the SEM image and XRD pattern of the catalyst after stability test were obtained. It can be seen the prismatic morphology preserves to a certain extent (Fig. S8†). However, the XRD pattern only exhibits the characteristic peaks of Ni foam, indicating the crystalline V-Co_3O_4 becomes amorphous (Fig. S9†). This phase transition behavior is common for OER catalysts due to the occurrence of the oxidation reaction.[35,36]

To further demonstrate the practical application of V-Co_3O_4-5, a full water splitting device using nickel foam (1 cm^2 with 100 μL catalyst ink) supported Pt/C and V-Co_3O_4-5 as the cathode and anode, respectively, was assembled (Fig. 5a). It can be seen that the combination using Pt/C and V-Co_3O_4-5 exhibits better catalytic activity than the traditional Pt/C and RuO_2 (Fig. 5b). Additionally, at a fixed current density of 50 mA cm^{-2} (H_2 yield of 0.35 ml min^{-1}), the generated hydrogen and oxygen are collected. Obviously, the H_2 and O_2 exhibit a volume ratio of 2 : 1 (Fig. 5c), and the faradaic efficiency approaches 100%, demonstrating that V-Co_3O_4-5 can be used for overall water splitting (Fig. 5d).[60,61]

The above electrochemical results indicate that V doping can effectively enhance the OER catalytic performance of Co_3O_4. As illustrated above, on one hand, V doping can modulate the electronic structure of Co, and induce the formation of more highly active sites. On the other hand, V doping could induce oxygen vacancies in low coordination sites (O_V) and improve the conductivity of V-Co_3O_4-5. Combining with the hollow structure that boosts mass transport, V-Co_3O_4-5 demonstrates superior catalytic performance and stability compared to most reported non-precious metal-based materials, showcasing significant potential for widespread applications.

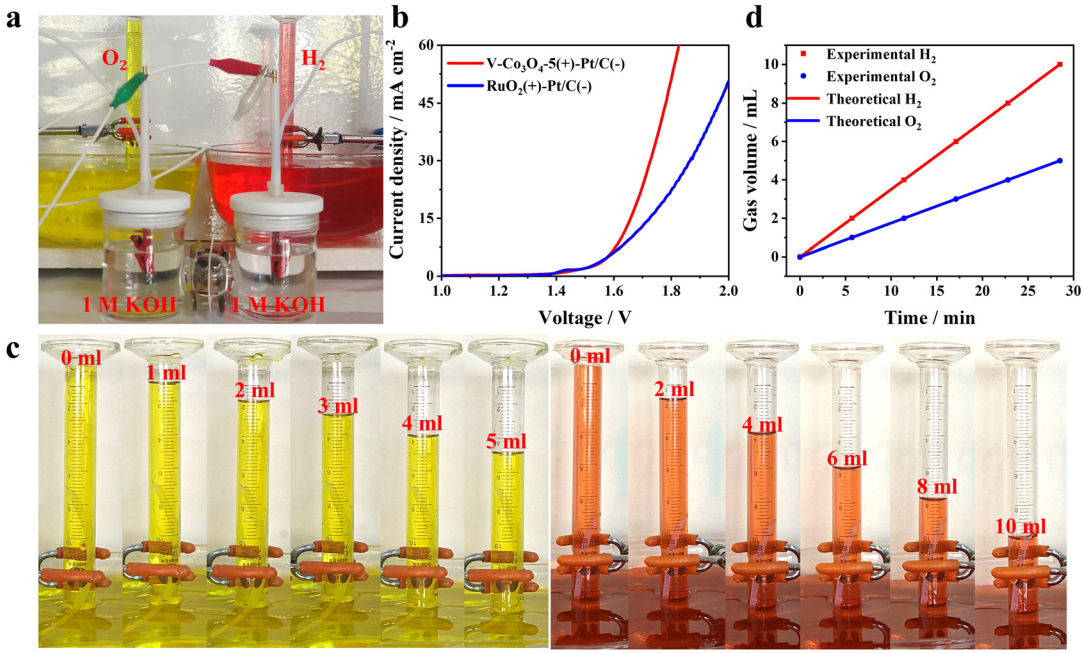

Fig. 5 (a) The assembled full water splitting device. (b) LSV curves of Pt/C-V-Co_3O_4-5 and Pt/C–RuO_2 for full water splitting. (c) The pictures of collected H_2 and O_2. (d) Faradaic efficiency of Pt/C–V-Co_3O_4-5 for overall water splitting.

4. Conclusions

In conclusion, we synthesized a series of V doped Co_3O_4 using sodium metavanadate as the source of vanadium. The doping of V can modify the electronic structure of Co_3O_4, therefore optimizing the binding energies between the catalyst and reactants or intermediates. In addition, the conductivity of the catalysts is also improved due to the formation of O_V. The optimized V-Co_3O_4-5 exhibits a small overpotential of 288 mV at 10 mA cm^{-2} with good stability. This work presents an alternative strategy for improving the catalytic performance of spinel catalysts.

Data availability

Data will be available on request.

Conflicts of interest

There are no conflicts to declare.

Acknowledgements

This work has been financially supported by the National Natural Science Foundation of China (No. 21902189), Training Plan of Young Backbone Teachers in Colleges and Universities of Henan Province (2023GGJS110), Natural Science Foundation of Henan Province (242300420208, 242300420036, and 252300420269), and Zhongyuan University of Technology Advantageous Discipline Strength Enhancement Program (GG202408).

References

1 Y. Li, J. Chen, Z. a. Wang and S. Chen, *ACS Appl. Nano Mater.*, 2024, **7**, 7555–7561.
2 H. Sun, X. Xu, H. Kim, Z. Shao and W. Jung, *InfoMat*, 2023, **6**, e12494.
3 L. Wang, J. Huang, Z. Huang, H. Li, T. Taylor Isimjan and X. Yang, *Chem. Eng. J.*, 2023, **472**, 144924.
4 K. Dashtian, S. Shahsavarifar, M. Usman, Y. Joseph, M. R. Ganjali, Z. Yin and M. Rahimi-Nasrabadi, *Coord. Chem. Rev.*, 2024, **504**, 215644.
5 H. Sun, X. Xu, H. Kim, W. Jung, W. Zhou and Z. Shao, *Energy Environ. Sci.*, 2023, **6**, e12441.
6 G. Chen, C. Wei, Y. Zhu and H. Huang, *EcoMat*, 2022, **5**, e12294.
7 Y. Li, X. Liu, J. Xu and S. Chen, *Small*, 2024, 2402846, DOI: **10.1002/smll.202402846**.
8 J. Zhang, X. Wang, F. Du, J. Wu, S. Xiao, Y. Zhou, H. Wu, Z. Shao, W. Cai and Y. Li, *Small*, 2024, **20**, 2400304.
9 F. Liu, C. Shi, X. Guo, Z. He, L. Pan, Z. F. Huang, X. Zhang and J. J. Zou, *Adv. Sci.*, 2022, **9**, 2200307.
10 P. Guo, G. Liu, J. Yin, H. Hu, E. Li, Y. Meng, H. Gao, W. Wang and Z. Li, *Fuel*, 2024, **355**, 129476.
11 R. Madhu, A. Karmakar, S. Kumaravel, S. S. Sankar, K. Bera, S. Nagappan, H. N. Dhandapani and S. Kundu, *ACS Appl. Mater. Interfaces*, 2021, **14**, 1077–1091.
12 H. Zhou, Y. Zhang, C. Shi, K. Yuan, R. Zhou, P. Zhao, Y. Qu and Y. Wang, *J. Colloid Interface Sci.*, 2024, **663**, 725–734.
13 S. Chen, J. Chen, J. Xu, Y. Yao, Z. Wang, W. Li and Y. Li, *Fuel*, 2025, **380**, 133272.
14 Y. Luo, Z. Zhang, M. Chhowalla and B. Liu, *Adv. Mater.*, 2022, **34**, 2108133.
15 X. Han, Y. Li, X. Wang, J. Dong, H. Li, S. Yin and J. Xia, *Int. J. Hydrogen Energy*, 2024, **51**, 769–776.
16 H. W. Choi, J. Kim, H.-S. Bang, K. Badawy, U. Y. Lee, D. I. Jeong, Y. Kim, K. Hamad, B. K. Kang, B. M. Weon, H.-S. Oh, N. Singh and D. H. Yoon, *J. Mater. Chem. A*, 2024, **12**, 7067–7079.
17 C. Chen, Z. Yang, W. Liang, H. Yan, Y. Tuo, Y. Li, Y. Zhou and J. Zhang, *J. Energy Chem.*, 2021, **55**, 345–354.
18 L. Zhang, X. Cao, C. Guo, A. Hassan, Y. Zhang and J. Wang, *J. Environ. Chem. Eng.*, 2023, **11**, 111373.
19 J. Zhang, Q. Wu, J. Song, C. Xu, S. Chen and Y. Guo, *Nano Energy*, 2024, **128**, 109923.
20 Z. Hou, F. Fan, C. Teng, L. Lv, L. Xu and Y. Du, *J. Alloys Compd.*, 2025, **1013**, 178510.
21 L. Li, R. Xu, X. Zhang, W. Wang, B. Yang, J. Yang, T. Zhou and P. Ma, *Ceram. Int.*, 2024, **50**, 45242–45250.
22 S.-F. Li, X. Li and D. Yan, *ACS Appl. Nano Mater.*, 2024, **7**, 13358–13366.
23 M. Ya, Y. Wang, J. Wang, G. Gao, X. Zhao, Y. Wei, Z. Geng, G. Li and L. Li, *ACS Sustainable Chem. Eng.*, 2023, **11**, 15451–15459.
24 H.-M. Xu, H.-R. Zhu, Z.-J. Zhang, C.-J. Huang, T.-Y. Shuai, Q.-N. Zhan and G.-R. Li, *Inorg. Chem.*, 2024, **63**, 3702–3711.
25 L. Tian, D. Zhong, T. Zhao, Y. Liu, L. Hao, Q. Fang, X. Lang, X. Zhao, G. Hao, G. Liu, J. Li and Q. Zhao, *J. Colloid Interface Sci.*, 2023, **646**, 452–460.
26 T. Wang, P. Wang, W. Zang, X. Li, D. Chen, Z. Kou, S. Mu and J. Wang, *Adv. Funct. Mater.*, 2021, **32**, 2107382.
27 J. Guo, G. Wang, S. Cui, B. Xia, Z. Liu and S.-q. Zang, *J. Colloid Interface Sci.*, 2023, **629**, 346–354.
28 Z. Shi, W. Yan, H. Feng, H. Song, Z. Fu, H. Zhuo, W. Chen and Y. Chen, *Electrochim. Acta*, 2024, **502**, 144871.
29 C.-Z. Yuan, S. Wang, K. San Hui, K. Wang, J. Li, H. Gao, C. Zha, X. Zhang, D. A. Dinh, X.-L. Wu, Z. Tang, J. Wan, Z. Shao and K. N. Hui, *ACS Catal.*, 2023, **13**, 2462–2471.
30 J. He, F. Liu, Y. Chen, X. Liu, X. Zhang, L. Zhao, B. Chang, J. Wang, H. Liu and W. Zhou, *Chem. Eng. J.*, 2022, **432**, 134331.
31 W. Sun, A. Meng, L. Wang, G. Li, J. Cui, Y. Sun and Z. Li, *J. Energy Chem.*, 2024, **94**, 29–40.
32 J. Zheng, X. Peng, Z. Xu, J. Gong and Z. Wang, *ACS Catal.*, 2022, **12**, 10245–10254.
33 J. Cao, D. Zhang, B. Ren, P. Song and W. Xu, *Energy Environ. Sci.*, 2024, **17**, 5911–5921.

34 T. Li, Z. Wang, L. Wang, M. Wang and Y.-Q. Liu, *Appl. Catal., B*, 2024, **352**, 123990.
35 Y. Wang, Y. Jiao, H. Yan, G. Yang, C. Tian, A. Wu, Y. Liu and H. Fu, *Angew. Chem., Int. Ed.*, 2022, **61**, 202116233.
36 Y. Wang, Y. Jiao, H. Yan, G. Yang, C. Tian, A. Wu, Y. Liu and H. Fu, *Angew. Chem.*, 2022, **134**, e202116233.
37 Y. Tang, J. Ding, W. Zhou, S. Cao, F. Yang, Y. Sun, S. Zhang, H. Xue and H. Pang, *Adv. Sci.*, 2023, **10**, 2206960.
38 L. Tian, Y. Liu, C. He, S. Tang, J. Li and Z. Li, *Chem. Rec.*, 2022, **23**, e202200213.
39 W. Liang, Y. Li, N. Zhang, J. Li, S. Li, Z. Wu and Y. Du, *Inorg. Chem.*, 2024, **63**, 14691–14698.
40 S. Chen, Y. Yao, J. Xu, J. Chen, Z. Wang, P. Li and Y. Li, *J. Colloid Interface Sci.*, 2024, **660**, 106–113.
41 S. Chen, J. Xu, J. Chen, Y. Yao, Z. Wang, P. Li, Y. Li and F. Wang, *J. Colloid Interface Sci.*, 2024, **658**, 230–237.
42 J. Chen, J. Xu, Y. Yao, S. Cui and S. Chen, *New J. Chem.*, 2023, **47**, 18532–18536.
43 J. Wang, H. Xuan, L. Meng, X. Liang, Y. Li, J. Yang and P. Han, *J. Colloid Interface Sci.*, 2023, **646**, 940–949.
44 Y. Li, Y. Zhou, Y. Ma, J. Xiong and S. Chen, *J. Alloys Compd.*, 2024, **1008**, 176709.
45 A. Behera, D. Seth, M. Agarwal, M. A. Haider and A. J. Bhattacharyya, *ACS Appl. Mater. Interfaces*, 2024, **16**, 17574–17586.
46 C. Wang, X. Wu, H. Sun, Z. Xu, C. Xu, X. Wang, M. Li, Y. Wang, Y. Tang, J. Jiang, K. Sun and G. Fu, *Energy Environ. Sci.*, 2025, **18**, 4276–4287.
47 J. Hu, X. Wang, Y. Zhou, M. Liu, C. Wang, M. Li, H. Liu, H. Li, Y. Tang and G. Fu, *Chem. Sci.*, 2025, **16**, 1837–1848.
48 L. Liu, Y. Zhang, J. Wang, R. Yao, Y. Wu, Q. Zhao, J. Li and G. Liu, *Int. J. Hydrogen Energy*, 2022, **47**, 14422–14431.
49 J. Qi, H. Wang, J. Lin, C. Li, X. Si, J. Cao, Z. Zhong and J. Feng, *J. Colloid Interface Sci.*, 2019, **557**, 28–33.
50 J.-Y. Xie, R.-Y. Fan, J.-Y. Fu, Y.-N. Zhen, M.-X. Li, H.-J. Liu, Y. Ma, F.-L. Wang, Y.-M. Chai and B. Dong, *Int. J. Hydrogen Energy*, 2021, **46**, 19962–19970.
51 C. Wang, H. Xu, Y. Wang, H. Shang, L. Jin, F. Ren, T. Song, J. Guo and Y. Du, *Inorg. Chem.*, 2020, **59**, 11814–11822.
52 X. Yu, X. Wang, S. Wu, J. Bai, P. He, F. Qin, Y. Yao and L. Ren, *J. Alloys Compd.*, 2023, **946**, 169383.
53 Z. Liu, Y. Cao, S. Wang, Z. Lu, J. Hu, J. Xie and A. Hao, *J. Alloys Compd.*, 2023, **965**, 171479.
54 L. Gao, X. Zhong, J. Chen, Y. Zhang, J. Liu and B. Zhang, *Chin. Chem. Lett.*, 2023, **34**, 108085.
55 J.-F. Qin, J.-H. Lin, T.-S. Chen, D.-P. Liu, J.-Y. Xie, B.-Y. Guo, L. Wang, Y.-M. Chai and B. Dong, *J. Energy Chem.*, 2019, **39**, 182–187.
56 Y. Huang, M. Li, F. Pan, Z. Zhu, H. Sun, Y. Tang and G. Fu, *Carbon Energy*, 2022, **5**, e279.
57 S. Raj, S. Anantharaj, S. Kundu and P. Roy, *ACS Sustainable Chem. Eng.*, 2019, **7**, 9690–9698.
58 K. Dai, N. Zhang, L. Zhang, L. Yin, Y. Zhao and B. Zhang, *Chem. Eng. J.*, 2021, **414**, 128804.
59 Y. Kong, D. Xiong, C. Lu, J. Wang, T. Liu, S. Ying, X. Ma and F.-Y. Yi, *ACS Appl. Mater. Interfaces*, 2022, **14**, 37804–37813.
60 J. Zhu, Q. Du, M. Arif Khan, H. Zhao, J. Fang, D. Ye and J. Zhang, *Appl. Surf. Sci.*, 2023, **623**, 156989.
61 S. Chen, J. Xu, J. Chen, J. Li, Y. Yao, Z. Wang and F. Wang, *J. Alloys Compd.*, 2024, **1003**, 175650.